



Catalytic oxidation of dichloromethane over Pt/CeO₂–Al₂O₃ catalysts

Qiu-Yan Chen, Na Li, Meng-Fei Luo, Ji-Qing Lu*

Key Laboratory of the Ministry of Education for Advanced Catalysis Materials, Institute of Physical Chemistry, Zhejiang Normal University, Jinhua 321004, China

ARTICLE INFO

Article history:

Received 12 June 2012

Received in revised form 18 August 2012

Accepted 20 August 2012

Available online 28 August 2012

Keywords:

CeO₂–Al₂O₃

Pt catalysts

Catalytic oxidation

Dichloromethane

Surface acidity

Redox property

ABSTRACT

A series of CeO₂–Al₂O₃ catalysts with different CeO₂ contents were prepared by a co-precipitation method, and supported Pt/CeO₂–Al₂O₃ catalysts were also prepared by an impregnation method. These catalysts were tested for catalytic oxidation of dichloromethane (CH₂Cl₂). It was found that these catalysts were active for the reaction, with a 100% conversion of CH₂Cl₂ obtained at 410 °C over a catalyst with 15% of CeO₂. Various characterization results such as ammonia temperature programmed desorption, hydrogen temperature programmed reduction suggested that the catalytic behaviors were synergistically influenced by surface acidity and redox property of the catalysts. An optimal combination of surface acidity and redox property in the catalyst resulted in a high activity. Moreover, the addition of Pt could further enhance the activity, due to the promotion of surface acidity by the introduction of chlorine species in the catalyst during the preparation using H₂PtCl₆ as the precursor and reducibility of the catalyst probably via the formation of Ce–Pt–O solid solution.

© 2012 Published by Elsevier B.V.

1. Introduction

Chlorinated volatile organic compounds (CVOs) are recognized to be hazardous to the environment and public health. These compounds are usually generated from a wide range of industrial processes, including the manufacture of herbicides, plastics and solvents. Dichloromethane (CH₂Cl₂) is a representative CVOs, which is harmful to the respiratory system and central nervous system of human [1]. Thus, elimination of CVOs emissions has been receiving much attention in recent decades. Among the technologies, catalytic combustion is regarded as one of the most promising technologies because of its low energy consumption, high efficiency and no associated pollution such as nitrogen oxides (NO_x) since it is operated at relatively low temperatures [2–4].

Catalysts applied in CVOs combustion could be generally categorized in three groups: transition metal oxides [5], supported noble metals (such as Pt and Pd) [6–8], and zeolites [9,10]. For example, we previously reported that CrO_x/Al₂O₃ catalysts were active for CH₂Cl₂ combustion [11], with a 18% Cr content catalyst having the highest activity. Recently, Gu et al. [12] prepared a CuMnO_x/Zr–Ti–Al catalyst and found that this catalyst was more active than the one without Zr modification, which could be attributed to the higher dispersion of CuMnO entities and the improvement of reducibility after Zr modification. In addition to the oxide catalysts, noble metal catalysts such as Pt and Pd are proven to be more active than the oxides, although these noble metals

may suffer deactivation during the reaction due to the poisoning of chlorine species [13]. Kim et al. reported that Pt–Pd bimetallic catalysts supported on γ-Al₂O₃ were very effective for benzene complete oxidation [14]. Very recently, Maupin et al. [15] studied the dichloromethane oxidation over a Pt/Al₂O₃ catalyst and concluded that the reaction followed a bifunctional mechanism, that is, CH₂Cl₂ disproportionation took place over alumina and oxidation over Pt.

It is well known that for the complete oxidation of CVOs, the performance of the catalysts correlates to several key factors such as surface acidity and redox properties, as the former is important for chemisorption of CVO molecules [16] and the latter is important for oxygen activation. In the latter case, CeO₂ appears to be very promising for the promotion of oxygen activation, due to its unique properties such as remarkable redox capability which could significantly ease the activation of oxygen during the reaction [17–23]. Moreover, the presence of CeO₂ as a support could help the dispersion of metals and prevent the sintering of noble metals [18]. Dai et al. [24] compared catalytic oxidation of 1,2-dichloroethane and ethyl acetate over ceria nanocrystals with well-defined crystal planes and found that the ceria nanorods possessed the highest activity due to its smaller crystallite size, more oxygen vacancies, higher OSC and mobility of oxygen than the nanocubes and nanooctahedrons. Abbasi et al. [25] conducted total oxidation of toluene, benzene and xylene over CeO₂ modified Pt/Al₂O₃ catalysts and concluded that the activity was due to the enhanced reducibility after the addition of Pt and CeO₂.

It seems that catalysts with a combination of surface acidity and redox property would be effective for CVOs combustion. As a typical acidic oxide, Al₂O₃ has been widely used in catalysis, especially

* Corresponding author. Fax: +86 579 2282595.

E-mail address: jiqinglu@zjnu.cn (J.-Q. Lu).

in the total oxidation of VOCs, as mentioned above [15,25]. Also, the choice of Al_2O_3 instead of other acidic materials such as zeolites lies in its cheap cost and easy synthesis. Moreover, as the CH_2Cl_2 molecule is very stable, the total oxidation of CH_2Cl_2 is challenging. Therefore, in this work, a series of $\text{CeO}_2\text{--Al}_2\text{O}_3$ oxides were synthesized and tested for complete oxidation of dichloromethane as a model reaction. Furthermore, Pt was supported on these oxides in order to promote the catalytic performance. Various characterizations were performed to correlate the catalytic behaviors with the natures of the catalysts.

2. Experimental

2.1. Catalyst preparation

$\text{CeO}_2\text{--Al}_2\text{O}_3$ catalysts were prepared by a co-precipitation method. A detailed process was as follows: an aqueous solution of $\text{Ce}(\text{NO}_3)_3 \cdot 6\text{H}_2\text{O}$ was mixed with an aqueous solution of $\text{Al}(\text{NO}_3)_3 \cdot 9\text{H}_2\text{O}$. Then an ammonia solution was drop-wise added to the mixture under vigorous stirring. The pH value of the solution was controlled at 8.0 ± 0.5 . The precipitation was aged for 6 h and separated by centrifugation from the mother liquor, washed several times with deionized water and then dried overnight at 120°C . The resulting solid was calcined at 500°C for 4 h with a heating rate of $10^\circ\text{C min}^{-1}$ to obtain the final $\text{CeO}_2\text{--Al}_2\text{O}_3$. The CeO_2 contents were about 5, 15, 27 and 59 wt% in the samples, and these catalysts were denoted as 5CeAlO, 15CeAlO, 27CeAlO and 59CeAlO, respectively. Reference supports Al_2O_3 and CeO_2 were prepared in a similar manner.

Supported Pt catalysts were prepared by an impregnation method. A known amount of platinum precursor ($\text{H}_2\text{PtCl}_6 \cdot 6\text{H}_2\text{O}$) was impregnated to the support. The solid was dried overnight at 120°C and then it was calcined at 500°C for 4 h to yield the final catalyst. The Pt contents in the catalysts ranged from 0.1 to 3.0 wt%.

2.2. Characterizations

The BET surface areas of the catalysts were measured by N_2 adsorption at liquid-nitrogen temperature (77 K), using a surface area analyzer (Quantachrome Autosorb-1). The catalysts were pretreatment at 120°C for 6 h in vacuum.

X-ray diffraction (XRD) patterns were recorded with a PANalytical X'Pert PRO MPD powder diffractometer using $\text{Cu K}\alpha$ radiation. The working voltage was 40 kV and the working current was 40 mA. The patterns were collected in a 2θ range from 10 to 90° , with a scanning speed of 0.15°s^{-1} . Cell parameter of CeO_2 was analyzed by full curve fitting using a JADE 6.5 software.

The morphology of the catalysts was observed by a scanning electron microscopy (SEM, Hitachi S-4800), which was operated at 1.0 kV. Detection of Pt particles in the supported catalysts was conducted on a transmission electron microscopy (TEM, JEOL JEM-2100F) operated at 120 kV.

H_2 temperature-programmed reduction ($\text{H}_2\text{--TPR}$) technique was used to measure the reducibility of the catalysts. 25 mg of the catalyst was placed in a quartz reactor, which was heated from 100 to 800°C with a heating rate of $10^\circ\text{C min}^{-1}$ under a mixture of 5% $\text{H}_2\text{--}95\% \text{N}_2$ (20 ml min^{-1}). The amount of H_2 consumption was determined by a gas chromatograph with a thermal conductivity detector (TCD), which was calibrated by the quantitative reduction of a known amount of CuO powder.

The acidic properties of the catalysts were studied by ammonia temperature programmed desorption ($\text{NH}_3\text{--TPD}$). 50 mg of the catalyst was pretreated in a flow of N_2 (20 ml min^{-1}) at 300°C for 0.5 h, and then was cooled down to 50°C . Afterwards, a flow of NH_3 (20 ml min^{-1}) was introduced to the reactor for 15 min, followed by

purging at 80°C for 0.5 h with a N_2 flow (20 ml min^{-1}) to remove the physisorbed NH_3 . Then the sample was heated from 80 to 600°C at a rate of $10^\circ\text{C min}^{-1}$, and the profile was recorded using a gas chromatograph (TECHTEMP GC 7890II) with a TCD detector.

The CH_2Cl_2 chemisorption experiments were carried out a home-made apparatus. 50 mg of the catalyst was pretreated in a flow of N_2 (20 ml min^{-1}) at 300°C for 0.5 h, and then was cooled down to 30°C . Then a flow of $\text{CH}_2\text{Cl}_2/\text{He}$ mixture (total flow rate = 20 ml min^{-1} , CH_2Cl_2 concentration = 3000 ppm) was introduced to the reactor for 15 min, followed by purging at 30°C for 0.5 h with a He flow (20 ml min^{-1}) to remove the physisorbed CH_2Cl_2 . Then the sample was heated from 30 to 500°C at a rate of $10^\circ\text{C min}^{-1}$, and the profile was recorded using a mass spectrometer (HIDEN, QIC-20) by monitoring $m/e = 97$ (CH_2Cl_2).

Dispersions of Pt in the catalysts were determined by CO chemisorption, which was carried out on a Quantachrome ChemBET-3000 instrument. The sample was placed in a quartz U-tube, and high-purity He (99.999%) was used as the carrier gas. The samples were reduced in a $\text{H}_2\text{--N}_2$ mixture (5 vol% H_2) stream at 300°C for 1 h and cooled down to 30°C in a pure He flow. Then pulses of CO were fed into the stream of carrier gas with a precision analytical syringe.

2.3. Activity test

Catalytic combustion of CH_2Cl_2 was carried out in a conventional fixed-bed reactor (i.d. = 9 mm). 1.0 g of the catalyst in 40–60 mesh was diluted into a volume of 2 ml with quartz sand, and then the mixture was loaded in the reactor. A thermal couple was placed in the middle of the catalyst bed to monitor the reaction temperature. A gaseous mixture of dichloromethane and air (moisture containing) was introduced to the catalysts, and the concentration of dichloromethane was 3000 ppm (GHSV = $15,000 \text{ h}^{-1}$). The reaction temperature was raised from R.T. to certain temperature with a heating rate of $10^\circ\text{C min}^{-1}$. After the reaction was held for 1 h at the temperature point, data analysis was conducted. The conversion of CH_2Cl_2 was analyzed by a gas chromatograph (Shimadzu, GC-14C) equipped with a FID detector. The outlet reaction mixture was neutralized by passing through a 0.1 M NaOH solution.

3. Results and discussion

3.1. Characterizations of the catalysts

Table 1 lists the physical properties of the catalysts. It can be seen that the surface areas of the catalysts are similar, except for the pure CeO_2 and 0.2Pt/ CeO_2 samples. For the CeAlO samples, the crystallite sizes of CeO_2 range from 11 to 15 nm, determined by the XRD results using the Scherrer equation. The cell parameters of these CeAlO samples slightly decrease with Ce content in the sample, with the 5CeAlO having a lattice parameter of 0.5415 nm and the 59CeAlO having a lattice parameter of 0.5412 nm (same as that of the pure CeO_2). This is due to the fact that the 5CeAlO sample has a CeO_2 crystallite size of 8.9 nm and that of the 59CeAlO sample is 14.9 nm, which causes a cell expansion because of the smaller CeO_2 particles in the 5CeAlO contain more defect sites than the larger ones. For the Pt containing catalysts, it is found that the addition of Pt in the 15CeAlO support does not change the surface area much, but significantly alters the cell parameter of CeO_2 . Note that the 0.1Pt/15CeAlO has a lattice parameter of 0.5401 nm while the 3.0Pt/59CeAlO has a lattice parameter of 0.5413 nm, which suggests that Pt species may incorporate into the CeO_2 matrix during the synthesis as the ionic radius of Pt^{2+} (0.086 nm) or Pt^{4+} (0.063 nm) is smaller than that of the Ce^{4+} (0.097 nm). Thus, the decreased cell parameter in the low Pt content samples (such as

Table 1
Physical properties of various catalysts.

Catalyst	BET (m ² g ^{−1})	CeO ₂ cell parameter (nm)	CeO ₂ crystal size (nm)	Pt dispersion ^a	Pt particle size ^b (nm)
Al ₂ O ₃	143	–	–	–	–
5CeAlO	174	0.5415	8.1	–	–
15CeAlO	168	0.5413	13.0	–	–
27CeAlO	163	0.5412	14.6	–	–
59CeAlO	105	0.5412	14.9	–	–
CeO ₂	43	0.5412	19.9	–	–
0.1Pt/15CeAlO	161	0.5401	13.4	0.52	2.0
0.2Pt/15CeAlO	159	0.5403	13.3	0.59	2.1
0.5Pt/15CeAlO	155	0.5405	13.2	0.56	2.2
1.0Pt/15CeAlO	163	0.5407	13.7	0.51	2.4
2.0Pt/15CeAlO	147	0.5408	13.5	0.50	2.5
3.0Pt/15CeAlO	160	0.5413	13.7	0.43	2.9
0.2Pt/CeO ₂	56	0.5412	19.8	0.61	2.1
0.2Pt/Al ₂ O ₃	183	–	–	0.63	2.0

^a Calculated based on CO chemisorption results.

^b Assuming that d (nm) = $1.24/D$ (dispersion).

the 0.1Pt/15CeAlO may due to the formation of Ce–Pt–O solid solution. Concerning the Pt dispersion, it is found that it does not change much at low Pt contents (<1.0 wt%), however, it decreases slightly with increasing Pt content in the catalyst. Consequently, Pt particle size increases gradually with Pt content in the catalyst.

Fig. 1 shows the XRD patterns of CeAlO and Pt/15CeAlO catalysts. It is found in Fig. 1a that the pure Al₂O₃ is amorphous, however, diffraction peaks due to cubic CeO₂ phase merge with increasing CeO₂ content in the sample. In addition, the intensities of the peaks become stronger with CeO₂ content, indicating growing crystallite size of CeO₂. Fig. 1b shows the diffraction peaks of the Pt containing catalysts, which are very similar to those of the supports. Note that no diffraction peaks due to Pt species are detected, implying that Pt species in the catalyst are highly dispersed. These are in good agreement with the CO chemisorption results (Table 1), because Pt particles with less than 3 nm in size can hardly be detected by XRD technique.

SEM images of CeAlO catalysts are shown in Fig. 2. It can be seen that all these samples consist nanosized aggregates. The morphology and microstructure of Pt-containing catalysts were investigated by TEM. Fig. 3 shows representative TEM images of the 0.2Pt/15CeAlO catalyst. The presence of Pt species (Pt⁰ and PtO) is confirmed by d -spacing measurements (Fig. 3a). Also, it is observed that the particle size of Pt species are about 2–4 nm, which is in well

consistent with the results obtained by CO chemisorptions. And the presence of CeO₂ and Al₂O₃ is also evidenced, as shown in Fig. 3b.

Fig. 4 shows the H₂-TPR profiles of the CeAlO and Pt/CeAlO catalysts. For the CeAlO catalysts (Fig. 4a), there are mainly reduction peaks at regions of 400–500 °C (α_1) and 600–700 °C (α_2). The α_1 peak could be assigned to the reduction of Ce⁴⁺ on the surface and the α_2 peak could be assigned to the reduction of Ce⁴⁺ in the bulk phase [26]. Fig. 4b shows the reduction profiles of the supported Pt catalysts. The reductions peaks locate at temperature regions of 150–280 °C (β_1), 250–350 °C (β_2) and 400–500 °C (β_3). The β_1 peak could be attributed to the reduction of surface Pt oxides [27], the β_2 peak could be attributed to the reduction of CeO₂ closely contacting with the Pt oxides, and the β_3 peak could be attributed to the surface Ce⁴⁺ that are far from the Pt oxides. Table 2 also lists the quantitative analysis results of H₂ consumptions of the catalysts. For the CeAlO catalysts, it is found that the H₂ consumption value increases with Ce content in the sample (except for the pure CeO₂), with the 5CeAlO having a H₂ consumption of 0.247 mmol g^{−1} and the 59CeAlO having a H₂ consumption of 0.709 mmol g^{−1}. However, note that the CeO₂ contents in these samples are different, therefore normalized ratios (defined as the H₂ consumption/Ce content in the sample) are also calculated. It is found that the 5CeAlO sample has the largest value (4.94) and the pure CeO₂ has the lowest one (0.072). This ratio reflects the reducibility of the samples and the changes in the values are due to the crystalline sizes of CeO₂ in the samples. As the 5CeAlO sample has a CeO₂ crystalline size of 8.1 nm and the pure CeO₂ has a crystalline size of 19.9 nm (Table 1), the small CeO₂ particles contain more defects sites than the large

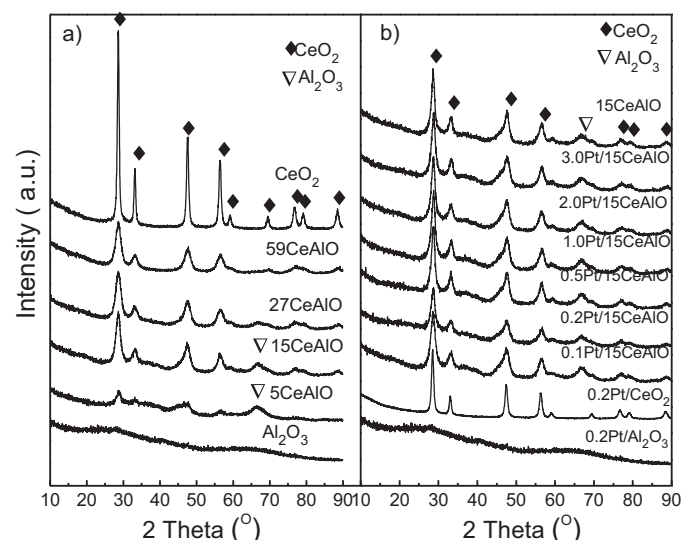


Fig. 1. XRD patterns of (a) CeAlO and (b) Pt/CeAlO catalysts.

Table 2
H₂ consumptions in various catalysts.

Catalyst	H ₂ consumption (mmol g ^{−1})		Actual/nominal ratio
	Nominal	Actual	
CeO ₂	–	0.072	0.072 ^a
5CeAlO	–	0.247	4.94 ^a
15CeAlO	–	0.336	2.24 ^a
27CeAlO	–	0.479	1.77 ^a
59CeAlO	–	0.709	1.20 ^a
Al ₂ O ₃	–	0	–
0.1Pt/15CeAlO	0.00512	0.144	28.1
0.2Pt/15CeAlO	0.0102	0.178	17.4
0.5Pt/15CeAlO	0.0256	0.221	8.63
1.0Pt/15CeAlO	0.0512	0.336	6.56
2.0Pt/15CeAlO	0.102	0.352	3.45
3.0Pt/15CeAlO	0.154	0.428	2.78
0.2Pt/CeO ₂	0.0102	0.181	17.7
0.2Pt/Al ₂ O ₃	0.0102	0.0116	1.13

^a Defined as H₂ consumption value/Ce content in the sample.

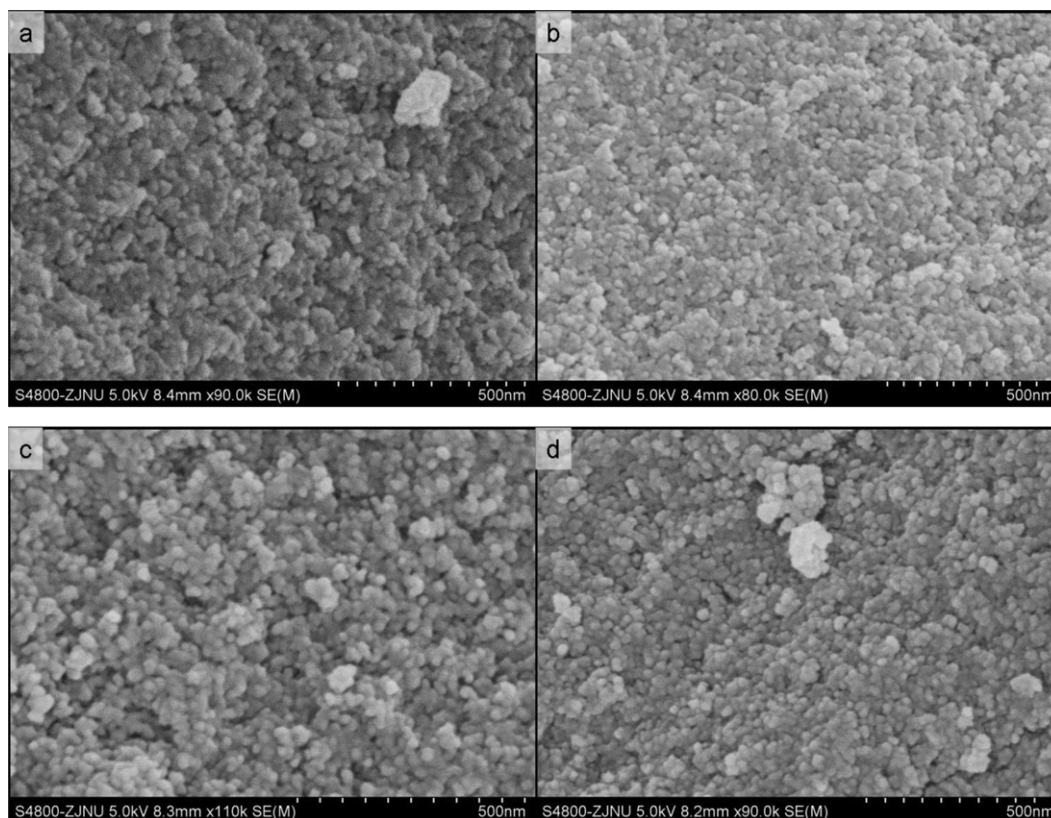


Fig. 2. SEM images of CeAlO catalysts: (a) 5CeAlO, (b) 15CeAlO, (c) 27CeAlO, and (d) 59CeAlO.

ones and thus are more reducible. For the Pt containing catalysts, it can be seen that the actual H_2 consumptions are much larger than the nominal values, indicating the simultaneous reduction of CeO_2 , due to a typical spillover effect. Also, it is found that the ratio of actual to nominal H_2 consumption increases with decreasing Pt content in the catalyst, suggesting stronger interaction between the Pt and CeO_2 and more enhanced redox property in the low Pt content catalysts compared to those with high Pt contents.

Fig. 5 shows the NH_3 -TPD profiles of the CeAlO and the supported Pt catalysts. For the Al_2O_3 containing supports (Fig. 5a), it is found that there is one broad peak centered at 200–250 °C, which could be assigned to Lewis acid sites on the Al_2O_3 surface. The pure

CeO_2 has negligible acidity. Also, the relative amount of surface acid sites (by integrating the peak area) decreases with CeO_2 content in the sample, from 23.9 for pure Al_2O_3 to 10.3 for the 59CeAlO sample. For the supported Pt catalysts, it is found that the position and features of the NH_3 desorption peak barely changes compared to that of the corresponding support, however, the amount of surface acidic sites is much larger than that of the supports and it increases with Pt content in the catalyst, which is due to the presence of residual Cl^- species in the catalyst because of the usage of H_2PtCl_6 precursor.

Fig. 6a shows the CH_2Cl_2 chemisorption on the catalysts. It can be seen that the largest amount of CH_2Cl_2 chemisorption is

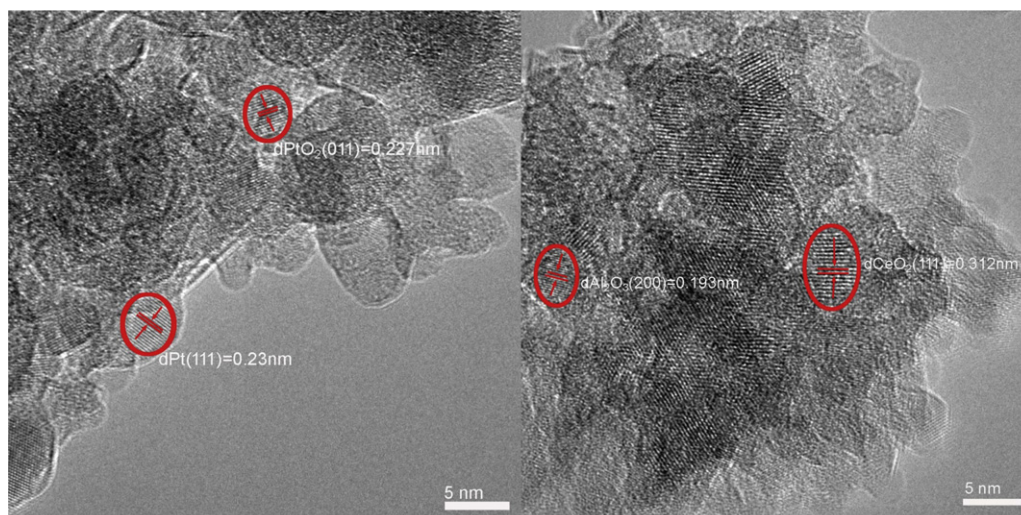


Fig. 3. TEM images of 0.2Pt/15CeAlO catalyst.

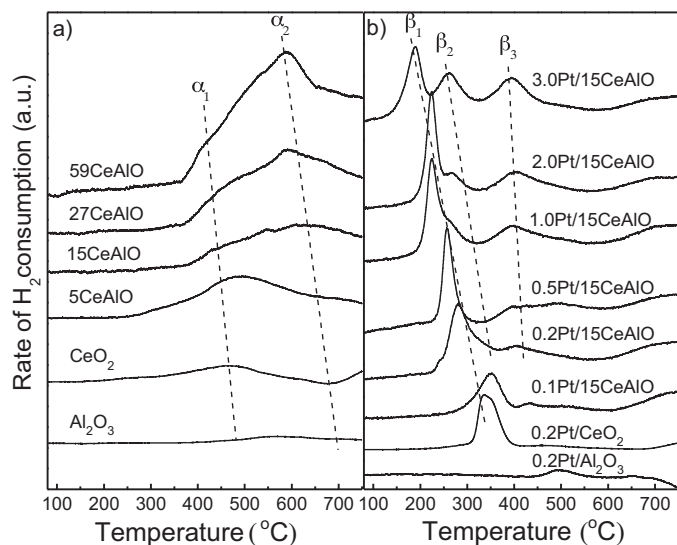


Fig. 4. H_2 -TPR profiles of (a) CeAlO and (b) Pt/CeAlO catalysts.

obtained on the bare Al_2O_3 , and the value decreases with increasing content of CeO_2 in the sample. Fig. 6b plots the surface acidity of the CeAlO samples versus the amount of chemisorbed CH_2Cl_2 , which shows an almost linear correlation between these values. This suggests that the surface acid sites of the samples provide centers for CH_2Cl_2 chemisorption.

3.2. Catalytic behaviors of the catalysts

Stability of the catalysts are firstly investigated, as shown in Fig. 7. It can be seen that the representative 15CeAlO and 2.0Pt/15CeAlO catalysts are quite stable during the reaction period (10 h) at the reaction temperature of 330 °C. Analyses of the spent catalysts such as BET and XRD (data not shown) reveal that there is little change in the physical properties of the catalysts. For example, the spent 15CeAlO and 2.0Pt/15CeAlO catalysts have surface areas of 160 and 142 $\text{m}^2 \text{g}^{-1}$ respectively, which are very close to those of the fresh ones (168 and 147 $\text{m}^2 \text{g}^{-1}$ respectively). This suggests that the catalysts structures remain unchanged during the reaction. Moreover, comparisons of H_2 -TPR and NH_3 -TPD profiles of the 15CeAlO, 2.0Pt/15CeAlO catalysts and their corresponding spent ones (Fig. 8) found that the reducibility and surface acidity of the

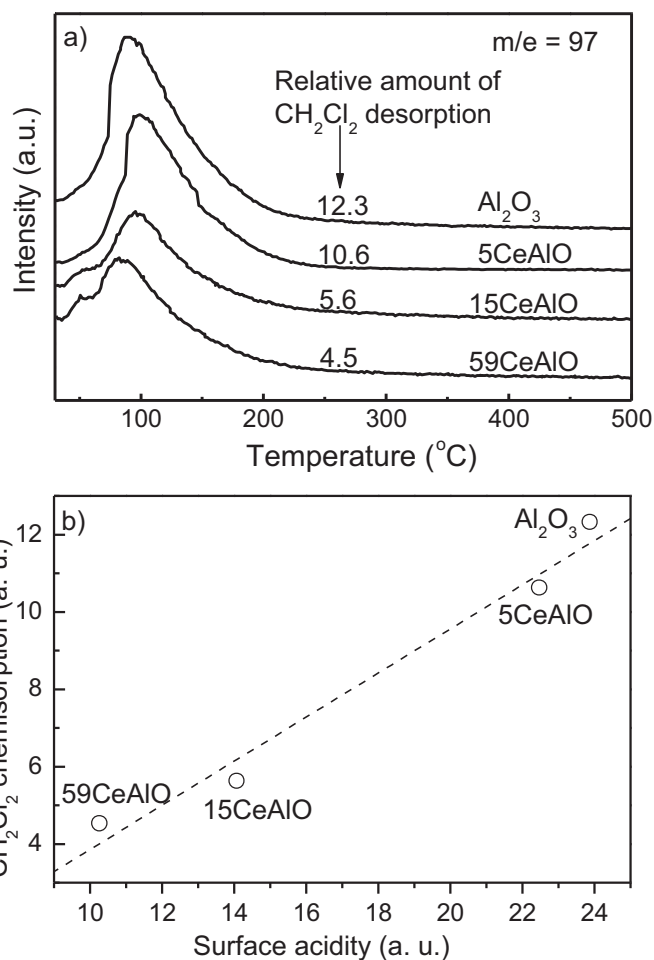


Fig. 6. (a) CH_2Cl_2 chemisorption on various CeAlO catalysts and (b) relationship between surface acidity and amount of chemisorbed CH_2Cl_2 .

catalysts do not change much after 10 h reaction, which indicates that the catalysts are quite stable and their surface properties (such as reducibility and surface acidity) remain intact. Fig. 9 presents the activities of the CeAlO and the supported Pt catalysts for CH_2Cl_2 oxidation. For CH_2Cl_2 oxidation over the CeAlO catalysts, the main reaction products are CO_x , HCl and Cl_2 . Chlorinated organic by-products such as CHCl_3 [28] are not detected, indicating that the

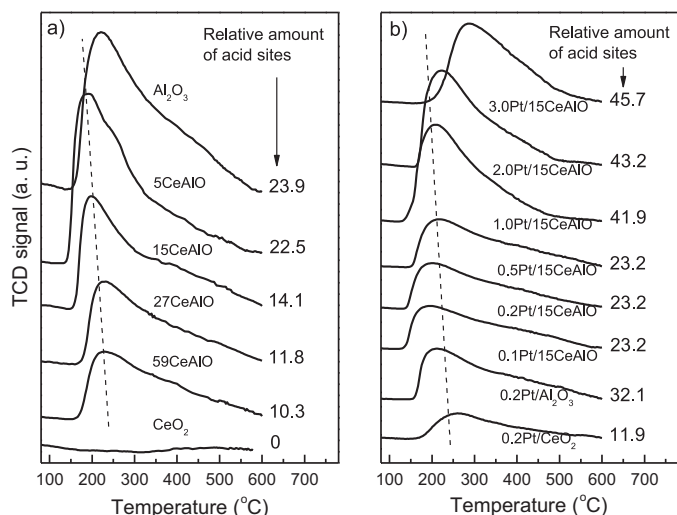


Fig. 5. NH_3 -TPD profiles of (a) CeAlO and (b) Pt/CeAlO catalysts.

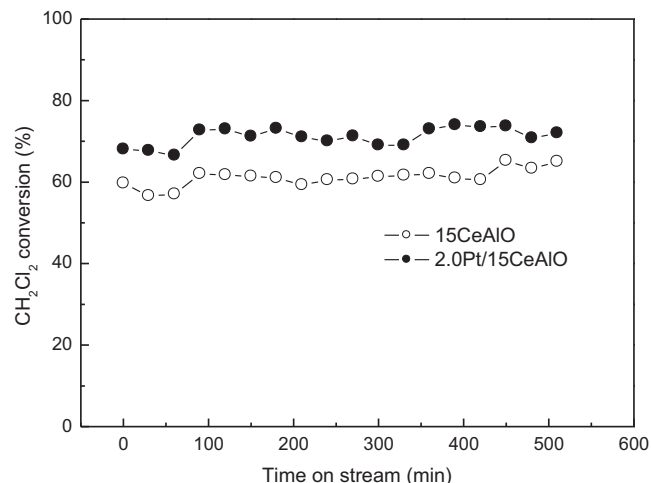


Fig. 7. Stability of representative catalysts. Reaction temperature was 330 °C.

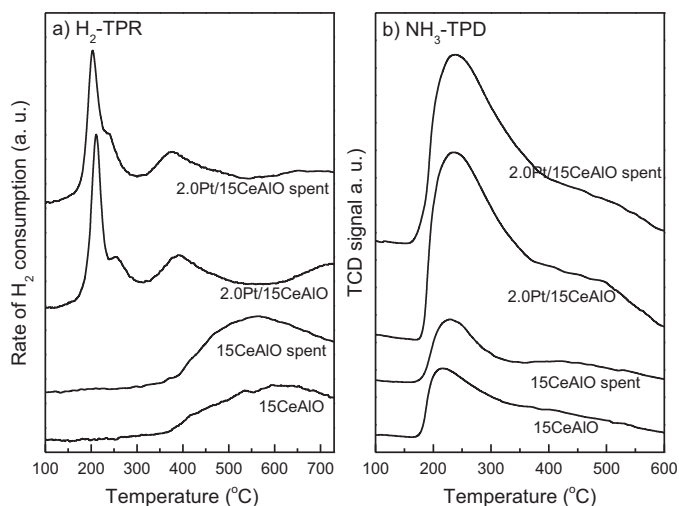


Fig. 8. Comparison of (a) H₂-TPR and (b) NH₃-TPD profiles of 15CeAlO, 2.0Pt/15CeAlO and their corresponding spent catalysts.

CH₂Cl₂ could be completely oxidized over these catalysts. However, the presence of other organic compounds such as formaldehyde (HCHO) could not be excluded because of the very low sensitivity of HCHO on the FID detector. Unfortunately, the selectivities of inorganic compounds such as CO_x, HCl and Cl₂ could not be qualitatively calculated due to the limitation of our reaction setup. From Fig. 9a, it can be seen that the Al-containing catalysts are much more active than the pure CeO₂. Among the CeO₂-doped Al₂O₃ catalysts, the low CeO₂ loading sample (5CeAlO) is less active than the pure Al₂O₃, while the medium CeO₂ loading samples (15CeAlO and 27CeAlO) are more active than the pure Al₂O₃. However, high content of CeO₂ in the sample (59CeAlO) results in suppressed activity. The 15CeAlO catalyst possesses the highest activity, with the lowest reaction

temperature for the conversion of 100% at 410 °C. Also, Fig. 9c plots the T50 (the temperature at which the conversion of CH₂Cl₂ is 50%) of the catalysts, which clearly shows that the 15CeAlO and 27CeAlO samples possess higher reactivity than the others, with T50 values of 320 and 324 °C, respectively. Fig. 9b shows the catalytic performance of the supported Pt catalysts. It can be seen that the Pt/15CeAlO catalysts are generally more active compared to the 15CeAlO support and Pt/CeO₂ or Pt/Al₂O₃ catalysts. In addition, catalysts with Pt contents of 0.2, 0.5, 1.0, 2.0 show better performance than those with Pt contents of 0.1 and 3%. Again, Fig. 9d shows that the 0.2Pt/15CeAlO catalyst is more active than the others, with a T50 of 312 °C. These results are comparable to those reported in literature. For example, Pitkääho et al. [29] conducted complete oxidation of CH₂Cl₂ over various Pt-containing monolith catalysts, and a T50 of about 350 °C was obtained over a Pt/Al–Ce catalyst, although the reaction conditions in their experiments were different from those employed in the current work (due to the unknown amount of catalyst weight used in the literature [29], the specific reaction rate could not be calculated).

The above results clearly indicate that the catalytic performance strongly depends on the chemical natures of the catalysts. For the CeAlO catalysts, it is found that the activity first increases and then decreases with the content of CeO₂ in the catalyst. This could be interpreted by the synergetic effects of surface acidity and redox properties of these samples. It is well known that the surface acid sites are effective for the adsorption of CH₂Cl₂ and the rupture of the C–Cl bond of chloroalkanes [16], thus the Al₂O₃ sample could chemisorb more CH₂Cl₂ molecules than others as it has the highest amount of surface acid sites (as evidenced in Figs. 5a and 6). The loss of surface acidity after CeO₂ addition may result in the inhibited activity, as the 5CeAlO is less active than the pure Al₂O₃. However, the enhanced activity obtained on the 15CeAlO and 27CeAlO could be attributed to the remarkably promoted redox properties of these catalysts, which may even compensate the negative effect of the surface acidity loss (Fig. 4). On the other hand, high

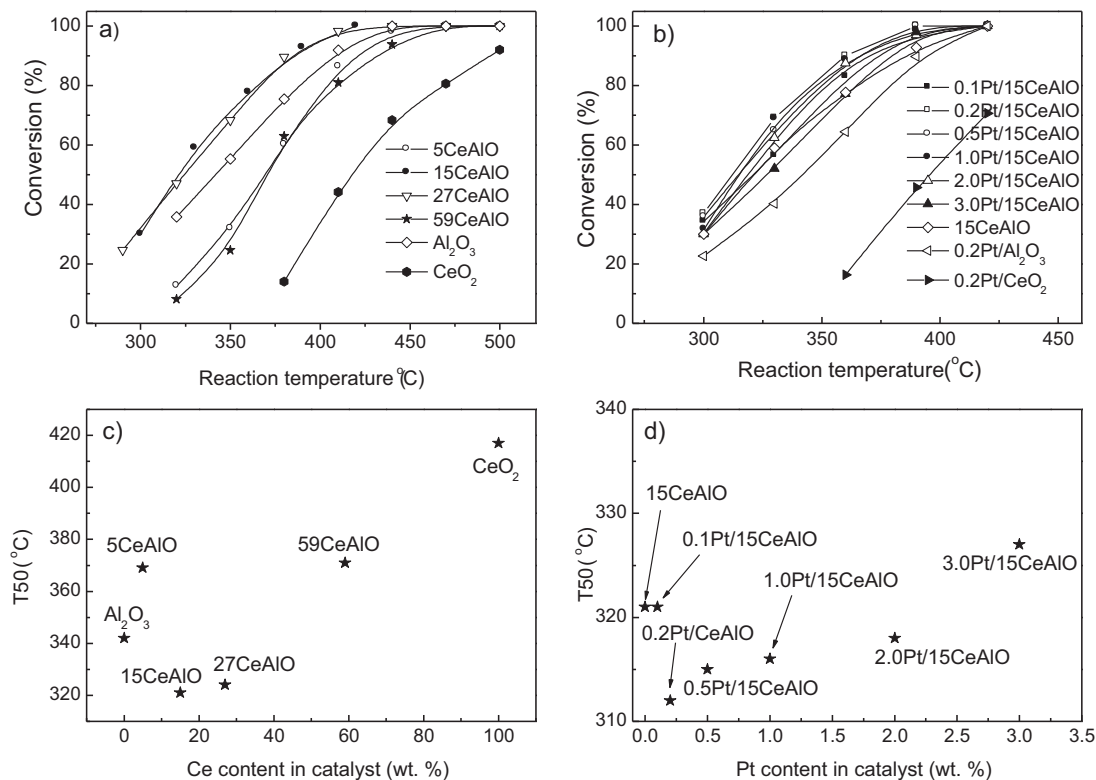


Fig. 9. CH₂Cl₂ oxidation over CeAlO and Pt/15CeAlO catalysts.

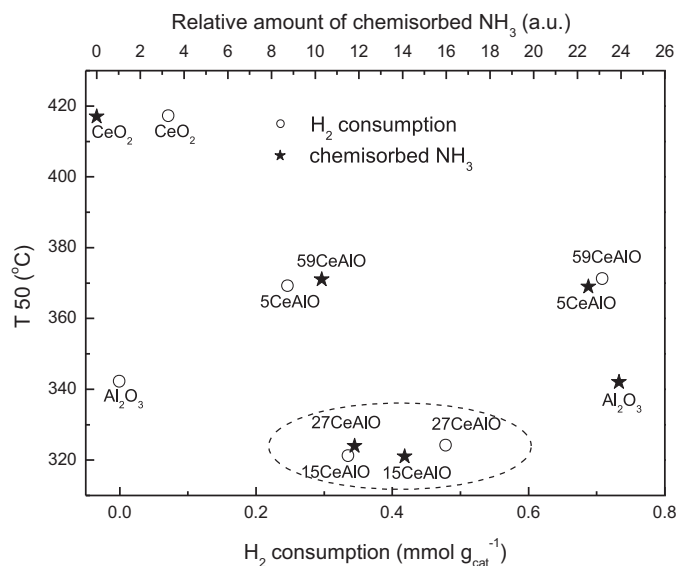


Fig. 10. Relationship between H_2 consumption, surface acidity and T50 of CeAlO catalysts.

content of CeO_2 in the sample (such as the 59CeAlO) could lead to the coverage of active sites by CeO_2 , and thus also inhibit the activity. This point could be confirmed by the sharp decline of surface area after high load of CeO_2 . For example, the surface area of the 59CeAlO ($105 \text{ m}^2 \text{ g}^{-1}$) is much lower than that of the pure Al_2O_3 ($143 \text{ m}^2 \text{ g}^{-1}$), indicating the blockage of Al sites by CeO_2 . Thus, the enhanced activity obtained on the 15CeAlO and 27CeAlO catalysts could be attributed to the surface acidity and the redox property. Similar conclusion was also obtained for catalytic oxidation of 1,2-dichloroethane (DCE) over CeO_2 modified USY zeolite catalysts, as the authors pointed out that both acidity and redox property played important roles in the DCE decomposition [30]. Fig. 10 demonstrates the relationship between H_2 consumption, surface acidity and T50 of the CeAlO catalysts. This figure again reveals that the catalytic performance of the catalyst correlates with the simultaneous contributions of surface acidity and redox property. Either samples with high surface acidity but low reducibility (such as 5CeAlO and Al_2O_3) or samples with high reducibility but low surface acidity (such as the 59CeAlO) are less active, while the samples with an optimal combination of these two facts (such as the 15CeAlO and 27CeAlO) are more active.

For the Pt containing samples, as the Pt contents in these catalysts are different, thus reaction rate in terms of turnover frequencies (TOFs) based on Pt dispersion reflect more intrinsic reactivity, as shown in Fig. 11. It is found that the TOFs decrease with Pt content in the catalyst. The highest TOF was obtained over the 0.1Pt/15CeAlO catalyst while the lowest TOF was obtained over the 3.0Pt/15CeAlO. The promoting effect of Pt addition on the catalytic activity (especially at low Pt loadings) may also be related to the synergetic effects of surface acidity and the redox property. NH_3 -TPD results (Fig. 5b) show that the amount of surface acid sites increases remarkably due to the introduction of chlorine to the supported Pt catalysts, which could explain the enhanced activities of these catalysts compared to that of the 15CeAlO. Note that the surface acidity of these catalysts does not follow the same trend as the activity (for example, the 3.0Pt/15CeAlO catalysts has the highest surface acidity but it is less active than the others), thus the redox properties of the catalysts after the Pt addition must be concerned. Fig. 12 demonstrates the correlation between the actual/nominal H_2 consumption ratio (obtained from Table 2) and the TOFs (obtained from Fig. 11). As the actual/nominal H_2 consumption ratio reflects the degree of surface reducibility, a higher

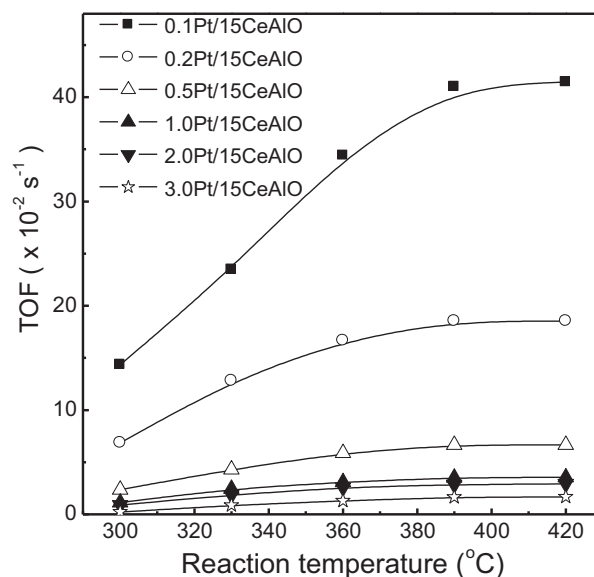


Fig. 11. TOFs of Pt/15CeAlO catalysts.

ratio implies a higher reducibility of the sample. It is interesting that the TOFs increase almost linearly with the ratio, which strongly suggests the surface reducibility plays very important role in this reaction, probably even more pronounced than the role of surface acidity. Such a promoted reducibility may result from the structural change of the catalyst via a strong interaction between the Pt species and the CeO_2 entities. As the analyses of the cell parameters of the Pt-containing samples (Table 1) clearly show that the cell parameters of the samples are smaller than that of the 15CeAlO support, which indicates the formation of Ce–Pt–O solid solution in these samples (especially for the low Pt content ones). Moreover, the cell parameter declines with decreasing Pt content, indicating that the relative amount of Ce–Pt–O solid solution in the low Pt content samples (e.g. the 0.1Pt/15CeAlO) is higher than that in the high Pt content ones (e.g. the 3.0Pt/15CeAlO). It is well known that such a CeO_2 -based solid solution provides more oxygen vacancies that are able to adsorb and activate O_2 (e.g. superoxide O_2^-) [31] and thus could be beneficial to the oxidation reaction. For example, our previous work [32] pointed out that a Au catalyst supported on a high surface area CeO_2 is more active for catalytic oxidation of formaldehyde compared to that on a low surface area

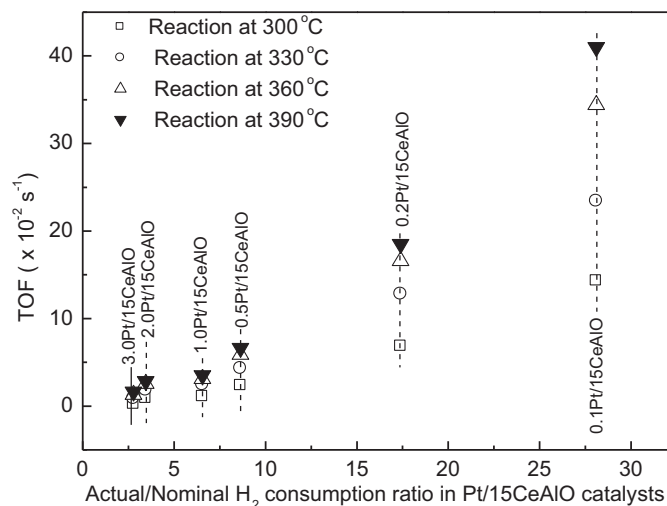


Fig. 12. Relationship between the H_2 consumption and TOFs of Pt catalysts.

CeO₂ due the former contained more oxygen vacancies than the latter. Thus, in the current case, the formation of Ce–Pt–O solid solution in the Pt containing catalysts could be responsible for the enhanced reducibility (and consequently for the enhanced reactivity). However, the origin of the difference in the relative amount of the Ce–Pt–O solid solution in various samples remains unclear at present, which needs further investigation in the future.

4. Conclusions

The CeO₂–Al₂O₃ catalysts were active for CH₂Cl₂ catalytic combustion, and the activity could be further promoted by the addition of Pt. It is found that both surface acidity and redox property of the catalyst are beneficial for the catalytic performance. Moreover, the addition of Pt in the catalyst enhanced the surface acidity and reducibility of the catalyst, which further promoted the activity.

Acknowledgment

This work is financially supported by Natural Science Foundation of China (Grant No. 21173195).

References

- [1] V.H. Vu, J. Belkouch, A. Ould-Dris, B. Taouk, *Journal of Hazardous Materials* 169 (2009) 758–765.
- [2] F. Bertinchamps, M. Treinen, N. Blangenois, E. Mariage, E.M. Gaigneaux, *Journal of Catalysis* 230 (2005) 493–498.
- [3] X.W. Su, L.Y. Jin, J.Q. Lu, M.F. Luo, *Journal of Industrial and Engineering Chemistry* 15 (2009) 683–686.
- [4] S. Chatterjee, H.L. Greene, Y.J. Park, *Journal of Catalysis* 138 (1992) 179–194.
- [5] Q.G. Dai, X.Y. Wang, G.Z. Lu, *Applied Catalysis B* 81 (2008) 192–202.
- [6] L.F. Wang, M. Sakurai, H. Kameyama, *Journal of Hazardous Materials* 154 (2008) 390–395.
- [7] S. Pitkääho, L. Matejova, S. Ojala, J. Gaalova, R.L. Keiski, *Applied Catalysis B* 113 (2012) 150–159.
- [8] A. Musialik-Piotrowska, *Catalysis Today* 119 (2007) 301–304.
- [9] A. Aranzabala, J.A. González-Marcosa, M. Romero-Sáez, J.R. González-Velasco, M. Guillemot, P. Magnoux, *Applied Catalysis B* 88 (2009) 533–541.
- [10] J.R. González-Velasco, R. López-Fonseca, A. Aranzabal, J.I. Gutiérrez-Ortiz, P. Steltenpohl, *Applied Catalysis B* 24 (2000) 233–242.
- [11] R. Ma, P. Hu, L. Jin, Y. Wang, J. Lu, M. Luo, *Catalysis Today* 175 (2011) 598–602.
- [12] Y. Gu, Y. Yang, Y. Qiu, K. Sun, X. Xu, *Catalysis Communications* 12 (2010) 277–281.
- [13] I.M. Freidel, A.C. Frost, K.J. Herbert, F.S. Meyer, J.C. Summers, *Catalysis Today* 17 (1993) 367–382.
- [14] H.S. Kim, T.W. Kim, H.L. Koh, S.H. Lee, B.R. Min, *Applied Catalysis A* 280 (2005) 125–131.
- [15] I. Maupin, L. Pinard, J. Mijoin, P. Magnoux, *Journal of Catalysis* 291 (2012) 104–109.
- [16] L. Intriago, E. Díaz, S. Ordóñez, A. Vega, *Microporous and Mesoporous Materials* 91 (2006) 161–169.
- [17] A. Parinyaswan, S. Pongstabodee, A. Luengnaruemitchai, *Journal of Hydrogen Energy* 31 (2006) 1942–1949.
- [18] S. Damyanova, J.M.C. Bueno, *Applied Catalysis A* 253 (2003) 135–150.
- [19] P. Djinić, J. Levec, A. Pintar, *Catalysis Today* 138 (2008) 222–227.
- [20] X.S. Huang, H. Sun, L.C. Wang, Y.M. Liu, K.N. Fan, Y. Cao, *Applied Catalysis B* 90 (2009) 224–232.
- [21] S. Bernal, G. Blanco, J.M. Pintado, J.M. Rodríguez-Izquierdo, M.P. Yeste, *Catalysis Communications* 6 (2005) 582–585.
- [22] D. Andreeva, R. Nedyalkova, L. Ilieva, M.V. Abrashev, *Applied Catalysis A* 246 (2003) 29–38.
- [23] R. Ramírez-López, I. Elizalde-Martínez, L. Balderas-Tapia, *Catalysis Today* 150 (2010) 358–362.
- [24] Q.G. Dai, H. Huang, Y. Zhu, W. Deng, S.X. Bai, X.Y. Wang, G.Z. Lu, *Applied Catalysis B* 117 (2012) 360–368.
- [25] Z. Abbasi, M. Haghighi, E. Faterhifar, S. Saedy, *Journal of Hazardous Materials* 186 (2011) 1445–1454.
- [26] X. Tang, B. Zhang, Y. Li, Y. Xu, Q. Xin, W. Shen, *Catalysis Today* 93–95 (2004) 191–198.
- [27] H. Lieske, G. Lictz, H. Spindler, J. Völter, *Journal of Catalysis* 81 (1983) 8–16.
- [28] B. Miranda, E. Díaz, S. Ordóñez, A. Vega, F.V. Díez, *Chemosphere* 66 (2007) 1706–1715.
- [29] S. Pitkääho, S. Ojalaa, T. Maunulab, A. Savimäkib, T. Kinnunenb, R.L. Keiski, *Applied Catalysis B* 102 (2011) 395–403.
- [30] Q. Huang, X. Xue, R. Zhou, *Journal of Hazardous Materials* 183 (2010) 694–700.
- [31] J. Guzman, S. Carrettin, A. Corma, *Journal of the American Chemical Society* 127 (2005) 3286–3287.
- [32] H.F. Li, N. Zhang, P. Chen, M.F. Luo, J.Q. Lu, *Applied Catalysis B* 110 (2011) 279–285.